MOLECULAR AND CELLULAR BIOLOGY, Dec. 2005, p. 11113–11121 Vol. 25, No. 24
0270-7306/05/$08.00+0 doi:10.1128/MCB.25.24.11113–11121.2005

Essential Role for Sphingosine Kinases in Neural and Vascular Development

Kiyomi Mizugishi,[1] Tadashi Yamashita,[1] Ana Olivera,[2] Georgina F. Miller,[3] Sarah Spiegel,[4] and Richard L. Proia[1]*

Genetics of Development and Disease Branch, NIDDK,[1] Molecular Immunology and Inflammation Branch, NIAMS,[2] and Division of Veterinary Resources,[3] National Institutes of Health, Bethesda, Maryland 20892, and Department of Biochemistry, Virginia Commonwealth University School of Medicine, Richmond, Virginia 23298[4]

Received 8 August 2005/Returned for modification 10 September 2005/Accepted 1 October 2005

Sphingosine-1-phosphate (S1P), an important sphingolipid metabolite, regulates diverse cellular processes, including cell survival, growth, and differentiation. Here we show that S1P signaling is critical for neural and vascular development. Sphingosine kinase-null mice exhibited a deficiency of S1P which severely disturbed neurogenesis, including neural tube closure, and angiogenesis and caused embryonic lethality. A dramatic increase in apoptosis and a decrease in mitosis were seen in the developing nervous system. $S1P_1$ receptor-null mice also showed severe defects in neurogenesis, indicating that the mechanism by which S1P promotes neurogenesis is, in part, signaling from the $S1P_1$ receptor. Thus, S1P joins a growing list of signaling molecules, such as vascular endothelial growth factor, which regulate the functionally intertwined pathways of angiogenesis and neurogenesis. Our findings also suggest that exploitation of this potent neuronal survival pathway could lead to the development of novel therapeutic approaches for neurological diseases.

Sphingosine-1-phosphate (S1P) is a signaling molecule that is crucial for the regulation of several diverse cellular events, including cell survival, growth, differentiation, motility, and calcium mobilization (29). Recently, numerous studies on S1P have demonstrated its importance in the development of the vascular system (1, 14, 16, 18), the heart (15), and immunity (2, 5, 21) by signaling through a family of G protein-coupled receptors designated $S1P_1$ to $S1P_5$. The S1P signaling pathway through S1P receptors induces activation of the protein kinase Akt, phosphatidylinositol 3-kinase, the small GTPase Rac, phospholipase C, and extracellular signal-regulated kinase, leading to cell survival and proliferation (11). In higher plants, S1P also plays an important role in calcium regulation and the control of guard cells (7).

Sphingosine kinase (SphK) is an enzyme that catalyzes the phosphorylation of sphingosine to form S1P. Two isoforms of mammalian *SphK* (*SphK1* and *SphK2*) have been cloned and characterized (13, 17). Recent studies revealed that overexpression of SphK2 suppressed cell growth and also markedly enhanced apoptosis in cultured cells (12, 19), in sharp contrast to findings for SphK1, which generally promoted cell survival and growth (26, 27).

Recently, we generated *SphK1* knockout mice to study the enzyme's physiological functions (3). The *SphK1*$^{-/-}$ mice were viable and fertile and lacked any obvious abnormalities, although total SphK activity was substantially, but not completely, reduced. These results raise the possibility that SphK1 and SphK2 might have redundant functions in mice and that SphK2 could compensate for a deficiency in SphK1 activity. To investigate the physiological functions of both isoforms, we generated *SphK2* knockout mice, as well as *SphK1*/*SphK2* double-knockout mice. Simultaneous deletion of both enzymes resulted in mice with undetectable levels of S1P. The studies on S1P-deficient mice described herein reveal a novel function for S1P signaling in neural development, in addition to its established role in vascular development.

* Corresponding author. Mailing address: Genetics of Development and Disease Branch, NIDDK, National Institutes of Health, Bldg. 10, Rm. 9N-314, 10 Center Dr., MSC 1821, Bethesda, MD 20892-1821. Phone: (301) 496-4391. Fax: (301) 496-0839. E-mail: proia@nih.gov.

MATERIALS AND METHODS

Generation of *SphK2* mutant mice. An 18.5-kb genomic DNA fragment of *SphK2* was cloned from a 129/Sv library and characterized. As shown in Fig. 1A, mouse *SphK2* consists of seven exons, with the coding region located in exons 3 to 7. A plasmid construct was created by replacing the region from the second half of exon 4 to the end of exon 7 with a *LacZ-Neo* cassette containing an internal ribosomal entry sequence. This targeting strategy should allow both disruption of the *SphK2* allele and analysis of *SphK2* expression in mice by creation of an *SphK2-LacZ* hybrid transcript driven by endogenous *SphK2* promoter elements. The herpes simplex virus thymidine kinase gene was located outside of the homologous sequence to prevent random integration. Correctly targeted embryonic stem cell clones were injected into C57BL/6 blastocysts, producing chimeric mice. Highly chimeric males were mated to C57BL/6 females, and then the progenitors were intercrossed.

Genotyping of *SphK1*, *SphK2*, and *$S1P_1$* mutant mice. Genotyping for the *$S1P_1$* and *SphK1* alleles was performed as previously described (3, 18). Genotyping for *SphK2* alleles was done by Southern blot or PCR analysis. For Southern blot analysis, SpeI-digested DNA was probed with a radiolabeled 3′ sequence that was located outside of the recombination site shown in Fig. 1A. For PCR analysis, genomic DNA was used as the template (40 cycles of 94°C for 30 s, 55°C for 30 s, and 72°C for 2 min) with primers P3 (5′-GCACCCAGTGTGAATCG AGC-3′), P4 (5′-TCTGGAGACGGGCTGCTTTA-3′), and P5 (5′-CGCTATC AGGACATAGCGTT-3′). Expected product sizes for the wild-type and targeted alleles were 680 and 310 bp, respectively.

RT-PCR. Total RNA was isolated with Trizol (Invitrogen). Total RNA (1 μg) was reverse transcribed with the SuperScript First-Strand Synthesis System for reverse transcription (RT)-PCR (Invitrogen) by following the manufacturer's instructions. PCR for *SphK2* alleles was performed with primers P1 (5′-ACCA CTTATGAGGAGAATCG-3′) and P2 (5′-CACCACGTGGTCCATACAGC-3′). Glyceraldehyde-3-phosphate dehydrogenase was used to monitor RNA recovery. The primer pairs used for amplification of the glyceraldehyde-3-phosphate dehydrogenase gene were from Applied Biosystems. Each PCR cycle consisted of 30 s of denaturation at 94°C, 30 s of annealing at 55°C, and 2 min of extension at 72°C.

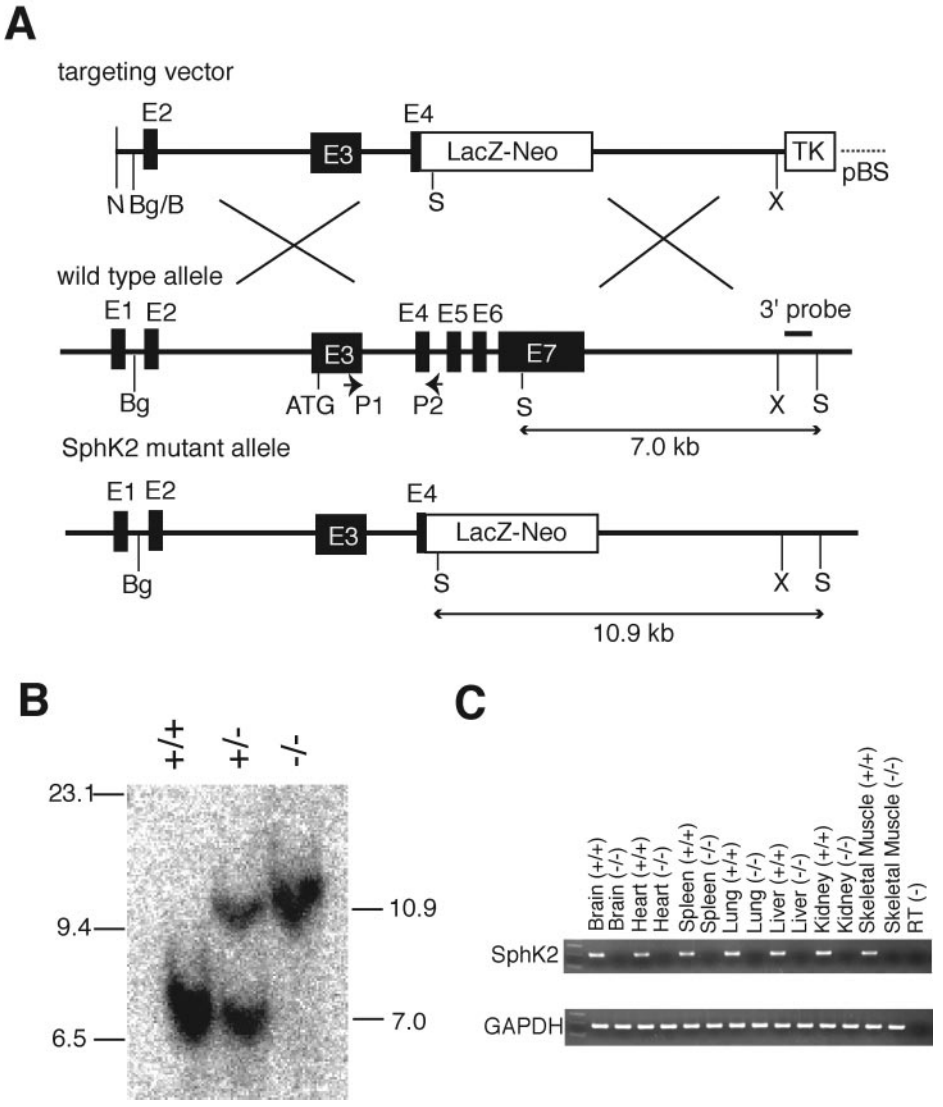

FIG. 1. Targeted disruption of the *SphK2* gene. (A) Schematic representation of the *SphK2* targeting strategy. The structure of the *SphK2* targeting vector is shown at the top, the mouse *SphK2* locus in the middle, and the predicted structure of the homologous recombined locus, with the location of the Southern probe, at the bottom. P1 and P2 were used for RT-PCR. B, BamHI; Bg, BglII; N, NotI; S, SpeI; X, XhoI; pBS; pBluescript vector. (B) Southern blot analysis of SpeI-digested genomic tail DNA from mice generated by *SphK2* heterozygous mating. The wild-type *SphK2* locus yielded a 7.0-kb SpeI band. The disrupted *SphK2* locus yielded a 10.9-kb SpeI band. (C) RT-PCR analysis of total RNA from adult tissues with primers P1 and P2. $SphK2^{+/+}$ RNA yielded the predicted 195-bp amplification product. No amplification product was detected from $SphK2^{-/-}$ RNA. GAPDH, glyceraldehyde-3-phosphate dehydrogenase.

Measurement of SphK activity. SphK activity was measured essentially as described previously (25). Homogenates from embryos at embryonic day 11.5 (E11.5) (15 μg of protein in sphingosine kinase buffer containing 50 mM Tris [pH 7.5], 10% glycerol, 1 mM β-mercaptoethanol, 1 mM EDTA, 1 mM sodium orthovanadate, 40 mM β-glycerophosphate, 15 mM NaF, 10 μg/ml each leupeptin and aprotinin, 1 mM phenylmethylsulfonyl fluoride, and 0.5 mM 4-deoxypyridoxine) were incubated with 50 μM sphingosine (prepared either in mixed micelles with Triton X-100 or in bovine serum albumin [BSA] complexes without Triton X-100), 10 μCi of [γ-^{32}P]ATP (1 mM), and 10 mM $MgCl_2$. Labeled lipids were extracted and resolved by thin-layer chromatography as described previously (25). Labeled S1P was quantified with a PhosphorImager.

Measurement of S1P levels. S1P levels in embryos at E11.5 were essentially measured as described previously (9, 13). Lipids from homogenates from embryos at E11.5 were extracted by adding 1 ml of 25 mM HCl–1 M NaCl, 1 ml of methanol, 1 ml of chloroform, and 100 μl of 3 N NaOH and phases separated. The aqueous phase containing S1P, devoid of sphingosine and the majority of phospholipids, was transferred to a siliconized glass tube. The organic phases were re-extracted with 1 ml of methanol–1 M NaCl (1:1, vol/vol) and the aqueous fractions combined. Mass levels of S1P in the pooled aqueous phases were determined exactly as described previously (13).

Measurement of sphingosine levels. Lipids from homogenates of embryos at E11.5 were extracted by adding 1 ml of 25 mM HCl–1 M NaCl, 1 ml of methanol, 1 ml of chloroform, and 100 μl of 3 N NaOH. After phase separation, the aqueous phase containing S1P was transferred to a siliconized glass tube and the organic phases were re-extracted with 1 ml of methanol–1 M NaCl (1:1, vol/vol). Aliquots of the lower organic phase containing sphingosine were dried under nitrogen and then resuspended in sphingosine kinase buffer with Triton X-100. Sphingosine converted to S1P was measured as described previously (9).

Histological analysis. Embryos were removed from the mother, fixed, and processed to be embedded in paraffin. Serial sections (5 μm) were made at 15- to 30-μm intervals and stained with hematoxylin and eosin (H&E). Immunostaining of vascular smooth muscle cells was performed with anti-smooth muscle α-actin antibody (Dako Cytomation). Paraffin sections were deparaffinized and rehydrated. Antigen retrieval was accompanied by 10-min incubation at 95°C in

Target Retrieval Solution (Dako Cytomation). Endogenous peroxidase activity was quenched by incubation with 3% hydrogen peroxide in water for 5 min. Specimens were incubated with anti-smooth muscle α-actin for 1 h at room temperature. After washing with phosphate-buffered saline (PBS), the peroxidase reaction was visualized with diaminobenzidine-hydrogen peroxide. Mitotic cells were reacted with 1:100-diluted anti-phospho histone H3 antibody (Upstate) overnight at 4°C. After that, they were reacted with 1:1,000-diluted, peroxidase-conjugated goat anti-rabbit immunoglobulin G (Upstate) for 30 min at room temperature and then visualized with diaminobenzidine-hydrogen peroxide.

Whole-mount immunostaining. Embryos were fixed in 4% paraformaldehyde in PBS at 4°C overnight. They were then dehydrated through a methanol series and stored in 100% methanol at −20°C. The embryos were bleached in 5% hydrogen peroxide-methanol for 1 h at room temperature and rehydrated through a methanol series to PBS plus 0.1% Triton X-100 (PBST). They were incubated in a blocking solution (4% BSA in PBST) twice, for 1 h each time. The embryos were incubated with rat anti-mouse CD31 antibody (anti-PECAM-1; PharMingen) diluted 1:10 in 4% BSA in PBST at 4°C overnight. Embryos were washed with 4% BSA in PBST at 4°C and then incubated with 1:100-diluted, peroxidase-conjugated goat anti-rat immunoglobulin G (Jackson ImmunoResearch) in 4% BSA in PBST at 4°C overnight. Peroxidase reaction was visualized with diaminobenzidine-hydrogen peroxide.

Whole-mount X-Gal staining. Embryos were fixed in 2% formaldehyde–2% glutaraldehyde in PBS for 1 h. They were washed in PBS and then incubated in PBS containing 5 mM $K_3Fe(CN)_6$, 5 mM $K_4Fe(CN)_6$, 2 mM $MgCl_2$, and 1 mg/ml 5-bromo-4-chloro-3-indolyl-β-D-galactopyranoside (X-Gal) at 37°C for 2 h to 12 h. Reactions were stopped by rinsing embryos with PBS, followed by further fixation in 4% formaldehyde.

Whole-mount in situ hybridization. In situ hybridization was performed essentially as described previously (31). The cDNA fragment corresponding to the entire open reading frame and the fragment including part of the C terminus and 3′ untranslated region of mouse *SphK1* were used as probes for hybridization. The two antisense probes produced the same staining pattern. Sense probes did not show any specific signals.

TUNEL assay. The terminal deoxynucleotidyltransferase-mediated dUTP-biotin nick end labeling (TUNEL) assay was performed with the Tdt-FragEL DNA Fragmentation Detection Kit (Calbiochem) according to the manufacturer's instructions.

Statistics. Data are expressed as means ± standard errors (SE). Results having P values of <0.01, or <0.05 by the paired Student t test, were considered significant.

RESULTS

Targeted disruption of *SphK2*. We created a null allele of *SphK2* by replacing it with a *LacZ-Neo* cassette (Fig. 1A). By intercrossing heterozygous mutant mice, viable homozygous *SphK2* mutant mice were obtained in the expected Mendelian ratio, indicating that this genotype was not associated with embryonic lethality. Correct targeting and deletion in the *SphK2* gene were confirmed by Southern blot (Fig. 1B) and PCR (data not shown) analyses of genomic DNA. The absence of *SphK2* transcripts from the deleted region in DNA from several tissues of adult homozygous mutant mice was confirmed by RT-PCR (Fig. 1C). Furthermore, no expression of SphK2 protein was detected in lysates of adult tissues derived from *SphK2* homozygous mutant mice, as determined by immunoblotting with an SphK2-specific antibody (data not shown). The levels of *SphK1* mRNA from several tissues (brain, heart, lung, liver, spleen, kidney, and skeletal muscle) of *SphK2* homozygous mutant mice were not significantly different from the levels of that from wild-type mice, as determined by real-time PCR (data not shown). The homozygous *SphK2* mutant mice were fertile and had normal longevity: histological analysis of major organs failed to reveal any obvious differences from wild-type mice.

***SphK1*$^{-/-}$ *SphK2*$^{-/-}$ mice are not viable.** The absence of abnormal gross or histological phenotypes in both *SphK1* and *SphK2* knockout mice led us to examine the effects of a combined loss of both *SphK1* and *SphK2*. Mice lacking one to four *SphK1* and *SphK2* alleles were generated by intercrossing *SphK1*$^{+/-}$ *SphK2*$^{+/-}$ mice. Offspring lacking one to three *SphK* alleles in any combination were indistinguishable from the wild type, but no animals lacking all four alleles were born, indicating that the *SphK1*$^{-/-}$ *SphK2*$^{-/-}$ genotype was lethal in these embryonic mice. To determine when *SphK1*$^{-/-}$ *SphK2*$^{-/-}$ mice die, *SphK1*$^{+/-}$ *SphK2*$^{-/-}$ mice were intercrossed and resulting embryos were examined. Between E9.5 and E10.5, *SphK1*$^{+/+}$ *SphK2*$^{-/-}$, *SphK1*$^{+/-}$ *SphK2*$^{-/-}$, and *SphK1*$^{-/-}$ *SphK2*$^{-/-}$ embryos were represented in the expected Mendelian ratio. *SphK1*$^{-/-}$ *SphK2*$^{-/-}$ embryos were grossly normal at E9.5; however, by E11.5 and E12.5, all embryos exhibited cranial hemorrhage and none survived beyond E13.5, indicating that expression of either SphK1 or SphK2 is essential for viability. Total SphK activity and S1P levels were measured in homogenates of whole embryos at E11.5. SphK activity and S1P levels were partially reduced in *SphK1*$^{-/-}$ *SphK2*$^{+/+}$ and *SphK1*$^{+/+}$ *SphK2*$^{-/-}$ embryos (Fig. 2A to C). In contrast, there was no detectable phosphorylation of sphingosine in *SphK1*$^{-/-}$ *SphK2*$^{-/-}$ embryos, irrespective of whether sphingosine was added in the presence of Triton X-100 (Fig. 2A), which stimulates SphK1 and inhibits SphK2, or as a complex with BSA, a condition in which both SphK1 and SphK2 are normally active (Fig. 2B). Accordingly, S1P levels in *SphK1*$^{-/-}$ *SphK2*$^{-/-}$ embryos were not detectable (Fig. 2C). Sphingosine levels in these embryos were not significantly different than levels in wild-type embryos (Fig. 2D), indicating that the lethal defects did not result from an increase in sphingosine. The expression of $S1P_1$, $S1P_2$, and $S1P_3$ mRNAs from *SphK1*$^{-/-}$ *SphK2*$^{-/-}$ embryos at E11.5 was not significantly changed from that from control embryos, as determined by real-time PCR (data not shown).

Vascular defects. By intercrossing *SphK1*$^{+/-}$ *SphK2*$^{-/-}$ mice, *SphK1*$^{-/-}$ *SphK2*$^{-/-}$ embryos were obtained in the expected Mendelian frequency, remaining grossly normal at E9.5. At E11.5, cranial hemorrhaging was evident in almost all *SphK1*$^{-/-}$ *SphK2*$^{-/-}$ embryos and 17% were not viable (Fig. 3A and B). Severely affected embryos had widespread hemorrhaging in areas other than the brain, such as the spinal cord and mandible (Fig. 3C). Some embryos had developed pericardial hemorrhages (Fig. 3D and H). Histological evaluation at E11.5 revealed that hemorrhaging was principally observed in the cranial mesenchymal region (Fig. 3E and F), sometimes accompanied by intraventricular hemorrhages in the brain (Fig. 3G). By E12.5, most of the *SphK1*$^{-/-}$ *SphK2*$^{-/-}$ embryos (70%) had died, apparently because of severe bleeding throughout the body. No embryos survived beyond E13.5.

The wall of the dorsal aorta was poorly developed in *SphK1*$^{-/-}$ *SphK2*$^{-/-}$ embryos at E11.5, compared to that of wild-type embryos (Fig. 3I and K). This finding led us to examine aortal covering by vascular smooth muscle cells, which is normally complete by E11.5. Visualization of smooth muscle α-actin revealed that covering of the aorta in *SphK1*$^{-/-}$ *SphK2*$^{-/-}$ embryos was patchy and incomplete (Fig. 3L), whereas aortal covering in the wild type was complete (Fig. 3J).

The blood vessel defects in *SphK1*$^{-/-}$ *SphK2*$^{-/-}$ embryos were further analyzed by electron microscopy. Endothelial

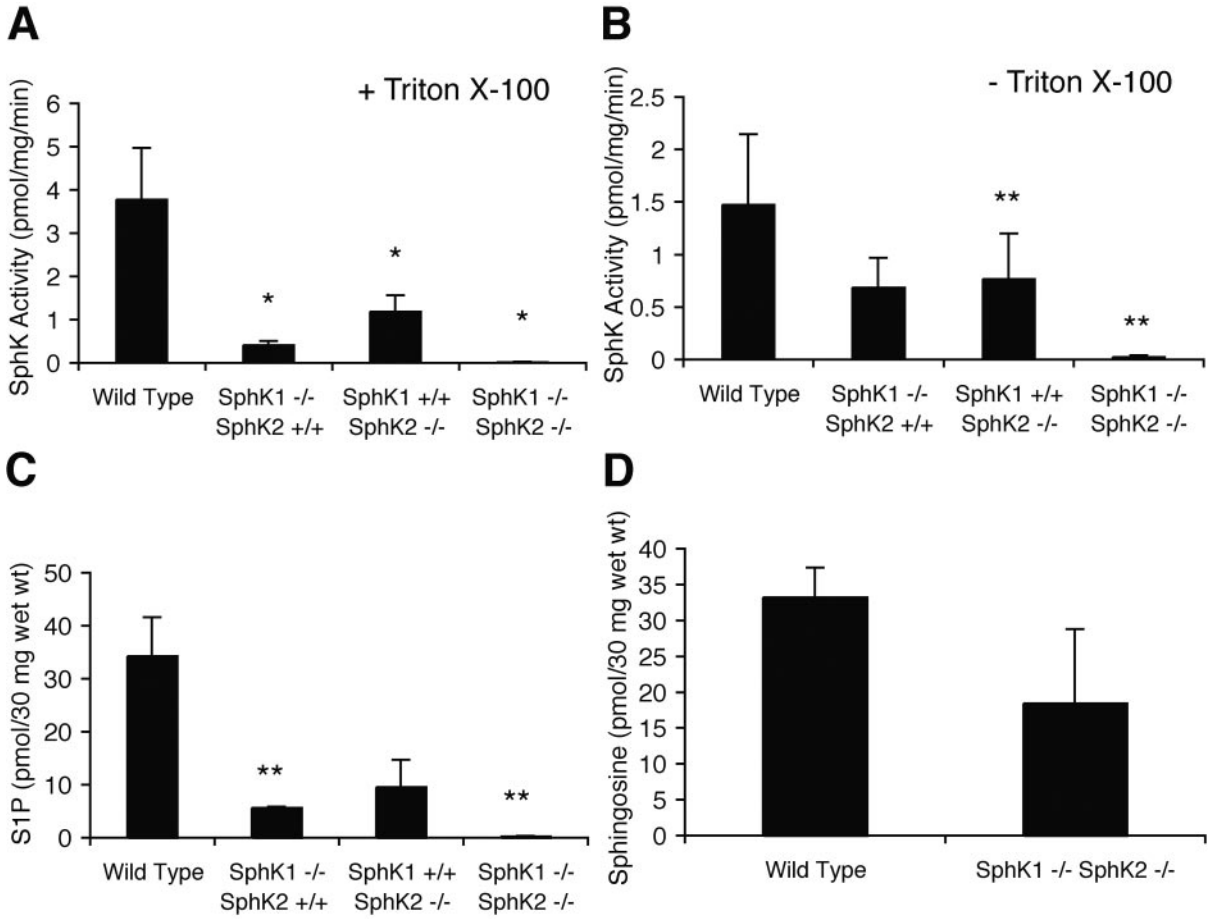

FIG. 2. Measurement of SphK activity and S1P levels in *SphK1 SphK2* combined mutants. (A and B) SphK enzymatic activity was determined in wild-type and $SphK1^{-/-}$ $SphK2^{+/+}$, $SphK1^{+/+}$ $SphK2^{-/-}$, and $SphK1^{-/-}$ $SphK2^{-/-}$ mutant embryos at E11.5. The assay was performed in the presence of Triton X-100 (A) or in BSA complexes without Triton X-100 (B). The data represent means ± SEs ($n = 3$; *, $P < 0.01$; **, $P < 0.05$ [paired *t* test compared with the wild type]). (C) S1P levels in wild-type and $SphK1^{-/-}$ $SphK2^{+/+}$, $SphK1^{+/+}$ $SphK2^{-/-}$, and $SphK1^{-/-}$ $SphK2^{-/-}$ mutant embryos at E11.5. The data represent means ± SEs ($n = 3$; **, $P < 0.05$ [paired *t* test compared with the wild type]) (D) Sphingosine levels in wild-type and $SphK1^{-/-}$ $SphK2^{-/-}$ mutant embryos at E11.5. The data represent means ± SEs ($n = 3$).

cells were severely defective in all blood vessels in the mesenchymal region of the head (Fig. 3O). Some vessels contained endothelial cells with vacuoles (Fig. 3P). In sharp contrast, endothelial cells in the neuroepithelium were intact in the mutants (data not shown). These findings are compatible with the histological localization of the main focus of bleeding in the mesenchyme. Wild-type endothelial cells were completely intact, having endothelial cell-cell junctions and supportive pericytes (Fig. 3M and N).

To further examine the vascular system in these mutants, whole-mount immunostaining was performed with an antibody directed against platelet endothelial cell adhesion molecule 1 (anti-PECAM-1). In $SphK1^{-/-}$ $SphK2^{-/-}$ embryos at E10.5, remodeling defects of blood vessels in the head were apparent; enlarged, dilated blood vessels (Fig. 3S) had formed, along with an aberrant anastomotic network (Fig. 3T).

Taken together, these results were strongly reminiscent of phenotypes observed in $S1P_1$ receptor-null embryos and in embryos carrying multiple S1P receptor mutations (1, 14, 18), substantiating that the effect of S1P receptors on vascular development is mediated by the S1P ligand.

NTDs. An unexpected finding in $SphK1^{-/-}$ $SphK2^{-/-}$ embryos was exencephaly, a cranial neural tube defect (NTD), at frequencies of 18% at E10.5, 13% at E11.5, and 20% at E12.5 (Fig. 4A to D and data not shown). However, no spina bifida was observed, indicating that the anterior neural tube closure was impaired in these embryos. To further investigate this phenomenon, we examined the expression of *SphK1* and *SphK2* in embryos at E10.5 by in situ hybridization and X-Gal staining, respectively. *SphK1* was expressed in the whole brain, with the highest levels in the telencephalon (Fig. 4E). The expression of *SphK2* was relatively ubiquitous, with the strongest signals detected in the limb buds, eyes, and branchial arches, and a weaker, but very apparent, level of expression in the telencephalon and spinal cord (Fig. 4F). These expression patterns overlapped that of the $S1P_1$ receptor, which was most prominent in the telencephalon and heart (18, 22) (Fig. 4G). No staining was detected in control embryos (Fig. 4H and data not shown). These overlapping expression patterns are consistent with the hypothesis that SphK1, SphK2, and the $S1P_1$ receptor are involved in neural development.

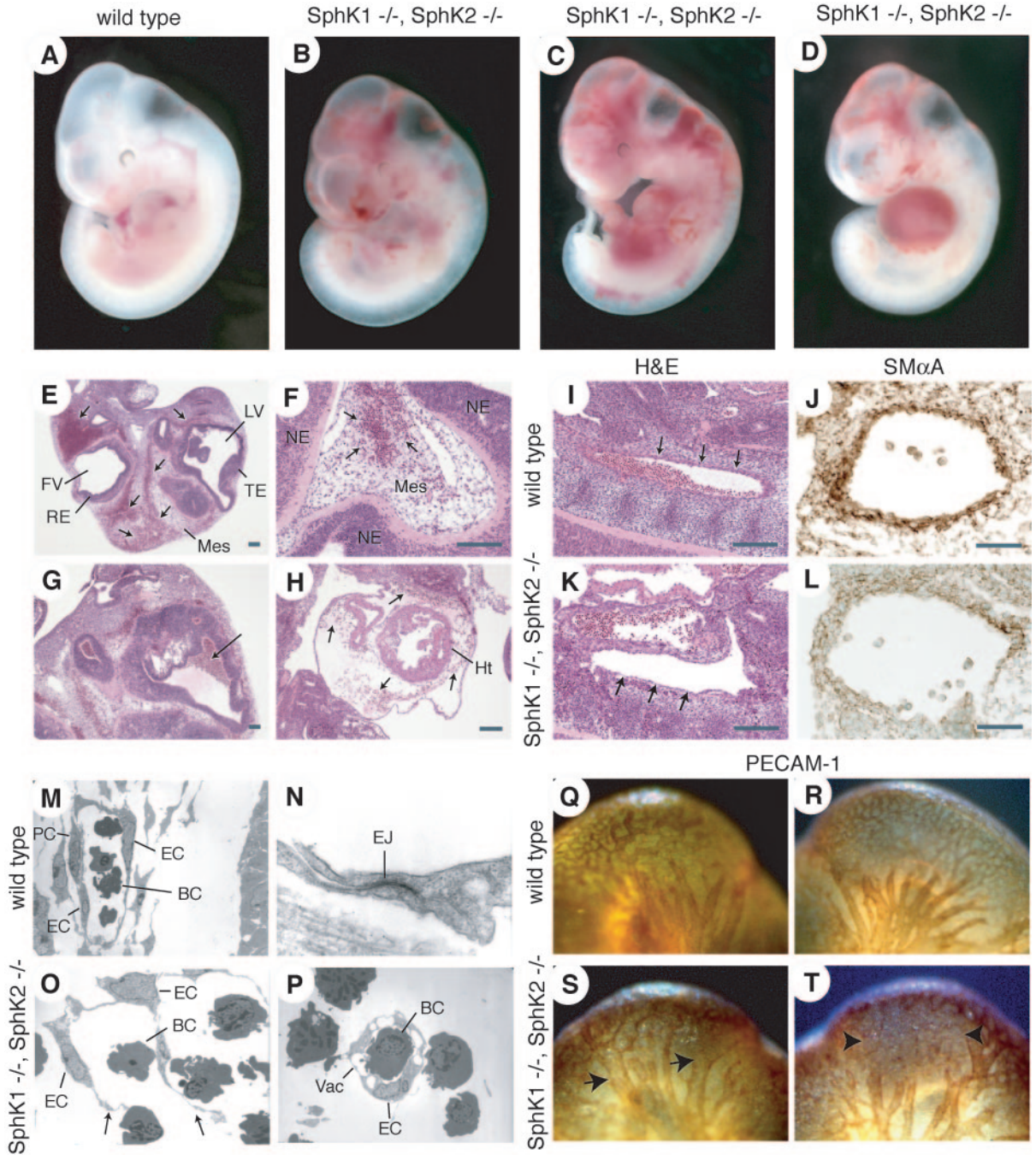

FIG. 3. Vascular defects in *SphK1*$^{-/-}$ *SphK2*$^{-/-}$ mutants. (A to D) Photomicrographs of E11.5 embryos. *SphK1*$^{-/-}$ *SphK2*$^{-/-}$ mutant embryos show hemorrhages in the brain (B to D), mandible (B), and spinal cord (C), sometimes along with enlargement of the cardiac profile (D). (E to H) H&E staining of sagittal sections from *SphK1*$^{-/-}$ *SphK2*$^{-/-}$ mutant embryos at E11.5. (E and F) Hemorrhage in the cranial mesenchymal region (arrows). (G) Intraventricular hemorrhage (arrow). (H) Pericardial hemorrhage (arrows). FV, fourth ventricle; Ht, heart; LV, lateral ventricle; Mes, mesenchyme; NE, neuroepithelium; TE, telencephalon; RE, rhombencephalon. (I to L) Vascular smooth muscle defects in *SphK1*$^{-/-}$ *SphK2*$^{-/-}$ mutants at E11.5. (I and K) H&E staining of sagittal sections of the dorsal aorta. The arrows in panel I and K indicate the wall of the aorta. (J and L) Transverse sections of the dorsal aorta stained with anti-smooth muscle α-actin (SMαA). (M to P) Electron microscopic analysis of blood vessels from the capillaries in the cranial mesenchymal region from E11.5 wild-type (M and N) and *SphK1*$^{-/-}$ *SphK2*$^{-/-}$ mutant (O and P) embryos. The arrows in panel O indicate broken endothelial cells. BC, blood cell; EC, endothelial cell; EJ, endothelial cell-cell junction; PC, pericyte; Vac, vacuole. Magnifications: M, ×1,600; N, ×50,000; O and P, ×2,000. (Q to T) Whole-mount immunostaining with anti-PECAM-1 antibody of blood vessels in the brains of E10.5 wild-type (Q and R) and *SphK1*$^{-/-}$ *SphK2*$^{-/-}$ mutant (S and T) embryos. Note the dilated blood vessels (arrows in panel S) and aberrant network (arrowheads in panel T). Scale bars represent 200 μm (E, F, G, H, I, and K) and 50 μm (J and L).

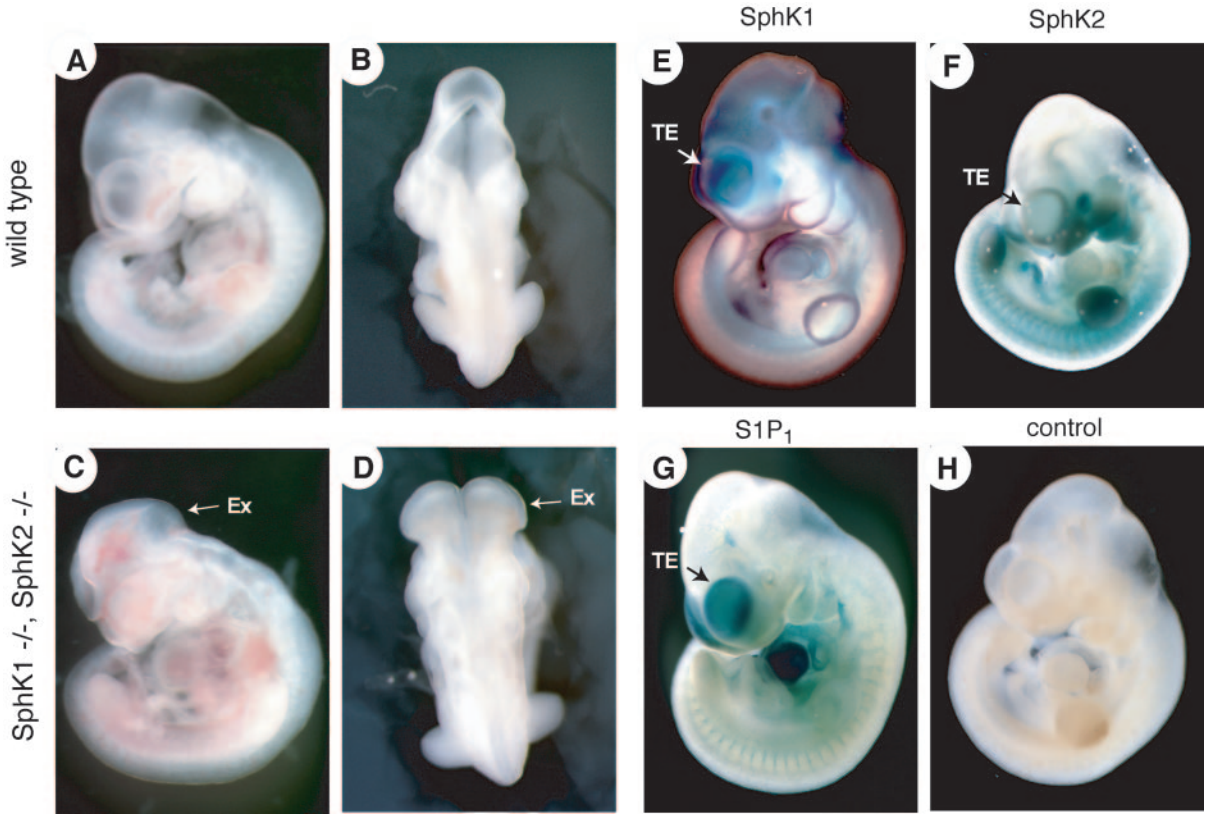

FIG. 4. NTDs in *SphK1*$^{-/-}$ *SphK2*$^{-/-}$ mutants. (A to D) Exencephaly in *SphK1*$^{-/-}$ *SphK2*$^{-/-}$ mutant embryos. (A and B) Wild-type control embryos at E10.5. (C and D) *SphK1*$^{-/-}$ *SphK2*$^{-/-}$ mutant embryos at E10.5. (A and C) Lateral view. (B and D) Dorsal view. Ex, exencephaly. (E to H) Expression of *SphK1*, *SphK2*, and *S1P*$_1$ in E10.5 embryos. (E) Whole-mount in situ hybridization for *SphK1* in a wild-type embryo. (F, G, and H) Whole-mount X-Gal staining of *SphK2*$^{-/-}$ and *S1P*$_1$$^{-/-}$ mutant and wild-type embryos, respectively. The *lacZ* reporter gene was inserted into the *SphK2* and *S1P*$_1$ loci. TE, telencephalon.

The effect of S1P on neural development is antiapoptotic and progrowth. We investigated the mechanism that underlies the NTDs in *SphK1*$^{-/-}$ *SphK2*$^{-/-}$ embryos. An imbalance between proliferation and cell survival in the neuroepithelium could potentially cause NTDs, leading to exencephaly (4, 6, 10, 28). S1P has been found to regulate cell growth and survival (8, 24). Therefore, we studied cell survival and growth in the neuroepithelium. Apoptosis was assessed in *SphK1*$^{-/-}$ *SphK2*$^{-/-}$ and wild-type embryos at E9.5 and E11.5 by the TUNEL assay. At E9.5, *SphK1*$^{-/-}$ *SphK2*$^{-/-}$ embryos showed enhanced apoptosis in the neuroepithelium in the mesencephalon and rhombencephalon, suggesting that this phenomenon may be responsible for the NTDs (Fig. 5A to D). A histological evaluation of the brain revealed a very thin, poorly developed wall of neuroepithelium, along with ventricular dilatation, in *SphK1*$^{-/-}$ *SphK2*$^{-/-}$ embryos at E11.5 (Fig. 5E and F). The neuroepithelial layer was irregularly shaped in the whole brain (Fig. 5G and H). Massive cell loss was also found in the neuroepithelial layer (data not shown). These defects were completely penetrative in *SphK1*$^{-/-}$ *SphK2*$^{-/-}$ embryos at E11.5, suggesting that the impairment of neural development is a general feature in *SphK1*$^{-/-}$ *SphK2*$^{-/-}$ embryos, whether or not exencephaly is present. *SphK1*$^{-/-}$ *SphK2*$^{-/-}$ embryos at E11.5 exhibited dramatically increased numbers of apoptotic cells in the neuroepithelium of almost all brain regions, but particularly in the telencephalon, correlating with the dramatic thinning of the neuroepithelial layer (Fig. 5I to K). Cell proliferation was assessed by anti-phospho-histone H3 immunostaining at E11.5. The total number of mitotic cells was significantly decreased in the telencephalon regions of the mutants' brains (Fig. 5L to N), while the number was not significantly changed in the diencephalon and rhombencephalon (Fig. 5N). Together, these results imply that S1P has antiapoptotic and progrowth effects during neural development.

Requirement of S1P$_1$ receptor for neural development. The expression pattern of the *S1P*$_1$ receptor implies a role in neural development. Histological analysis of S1P$_1$ receptor-null (*S1P*$_1$$^{-/-}$) embryos at E12.5 revealed massive cell loss in the forebrain (Fig. 6A and B). TUNEL analysis showed that apoptotic cells were significantly more numerous in the neuroepithelial layers of the telencephalon and diencephalon regions in *S1P*$_1$$^{-/-}$ embryos at E12.5 (Fig. 6C to E). A smaller, but significant, increase in cell death was observed in earlier E11.5 *S1P*$_1$$^{-/-}$ embryos, when bleeding was not evident (data not shown). Cell proliferation was also affected in *S1P*$_1$$^{-/-}$ embryos at E12.5; mitotic cell numbers were significantly decreased in the telencephalon regions (Fig. 6F to H). These results indicate that the effect of S1P on neural development is likely mediated, at least in part, by signaling from the S1P$_1$ receptor.

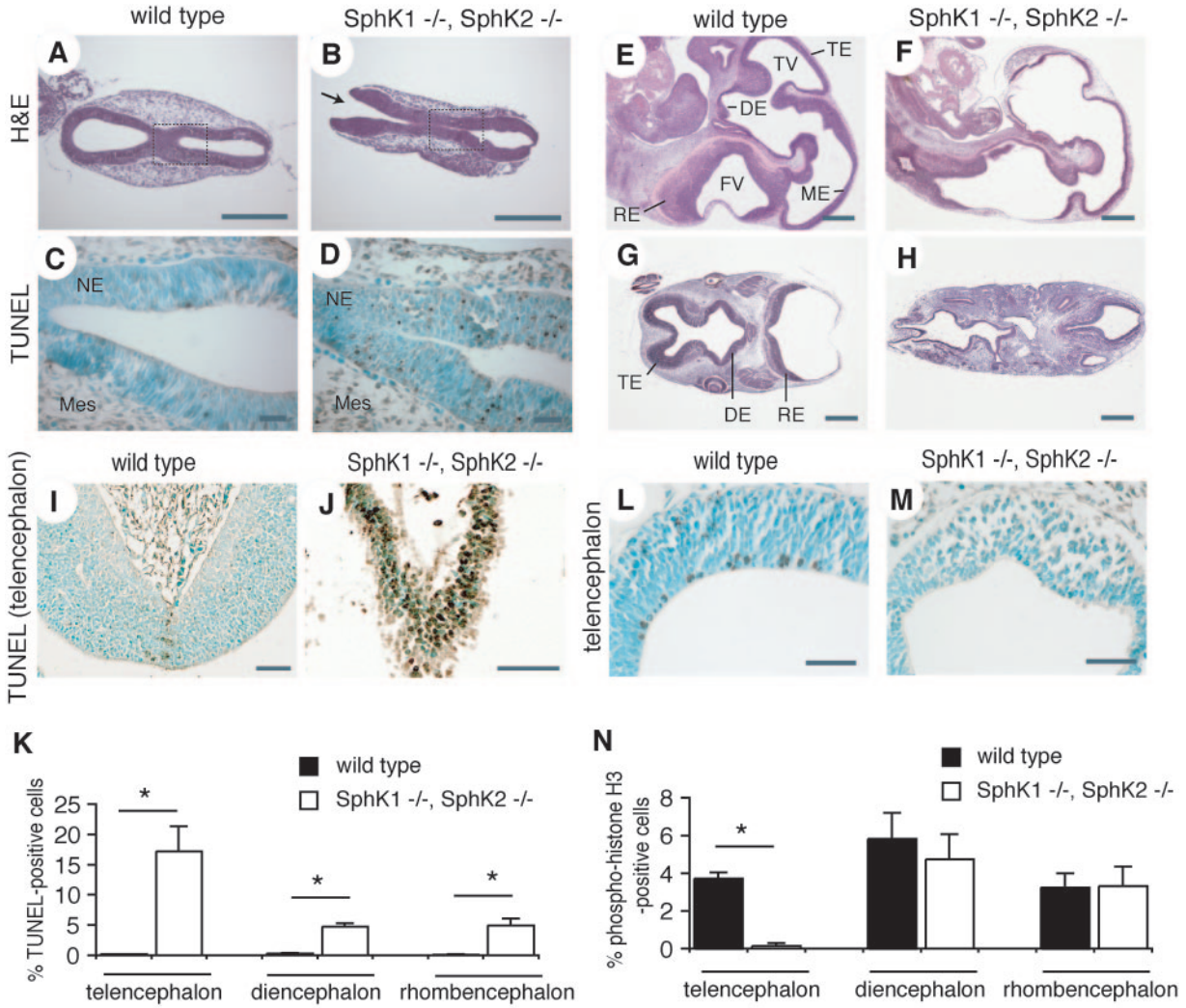

FIG. 5. Increased cell death and decreased cell proliferation in *SphK1*$^{-/-}$ *SphK2*$^{-/-}$ mutants. (A and B) H&E staining of transverse sections from wild-type (A) and *SphK1*$^{-/-}$ *SphK2*$^{-/-}$ mutant (B) embryos at E9.5. An arrow in panel B indicates an NTD. (C and D) TUNEL assay of wild-type (C) and *SphK1*$^{-/-}$ *SphK2*$^{-/-}$ mutant (D) embryos at E9.5. The boxed areas in panels A and B are shown, respectively. NE, neuroepithelium; Mes, mesenchyme. (E to H) H&E staining of sections from wild-type (E and G) and *SphK1*$^{-/-}$ *SphK2*$^{-/-}$ mutant (F and H) embryos at E11.5. (E and F) Sagittal sections. (G and H) Transverse sections. DE, diencephalon; FV, fourth ventricle; ME, mesencephalon; RE, rhombencephalon; TE, telencephalon; TV, third ventricle. (I and J) TUNEL assay of wild-type (I) and *SphK1*$^{-/-}$ *SphK2*$^{-/-}$ mutant (J) embryos at E11.5. The telencephalon is shown. (K) Percentage of TUNEL-positive cells ($n = 5$ matched pairs; *, $P < 0.01$ [paired t test]). (L and M) Immunostaining with anti-phospho-histone H3 of wild-type (L) and *SphK1*$^{-/-}$ *SphK2*$^{-/-}$ mutant (M) embryos at E11.5. The telencephalon is shown. (N) Percentage of phospho-histone H3-positive cells ($n = 4$ matched pairs; *, $P < 0.01$ [paired t test]). Scale bars represent 500 μm (A, B, E, F, G, and H) and 50 μm (C, D, I, J, L, and M).

DISCUSSION

We demonstrate that S1P signaling during embryonic development is critical for neurogenesis, in addition to angiogenesis. Simultaneous disruption of the two known sphingosine kinase genes in mice, *SphK1* and *SphK2*, resulted in a deficiency of S1P, which severely disturbed both angiogenesis and neurogenesis, including neural tube closure, followed by embryonic lethality. S1P levels were also partially reduced in *SphK1*$^{-/-}$ *SphK2*$^{+/+}$ and *SphK1*$^{+/+}$ *SphK2*$^{-/-}$ embryos, suggesting that S1P levels are regulated by both SphK1 and SphK2 during development. In contrast, S1P levels in most tissues from *SphK1* single-mutant mice were not markedly decreased, although there was a significant reduction (50%) of the S1P level in serum (3). We did not detect a significant reduction of the S1P level in serum from *SphK2* single-mutant mice (6 to 8 weeks old).

The vascular defects were expected, since mice with disrupted S1P receptor genes had shown similar defects in vascular development (1, 14, 18). Thus, our findings provide confirmation that the effect of S1P receptors on vascular development is mediated via S1P signaling. In contrast to the vascular defects, neural defects were unexpected and provided an entirely novel insight into the function of S1P signaling during development. About 15 to 20% of *SphK*-null mice ex-

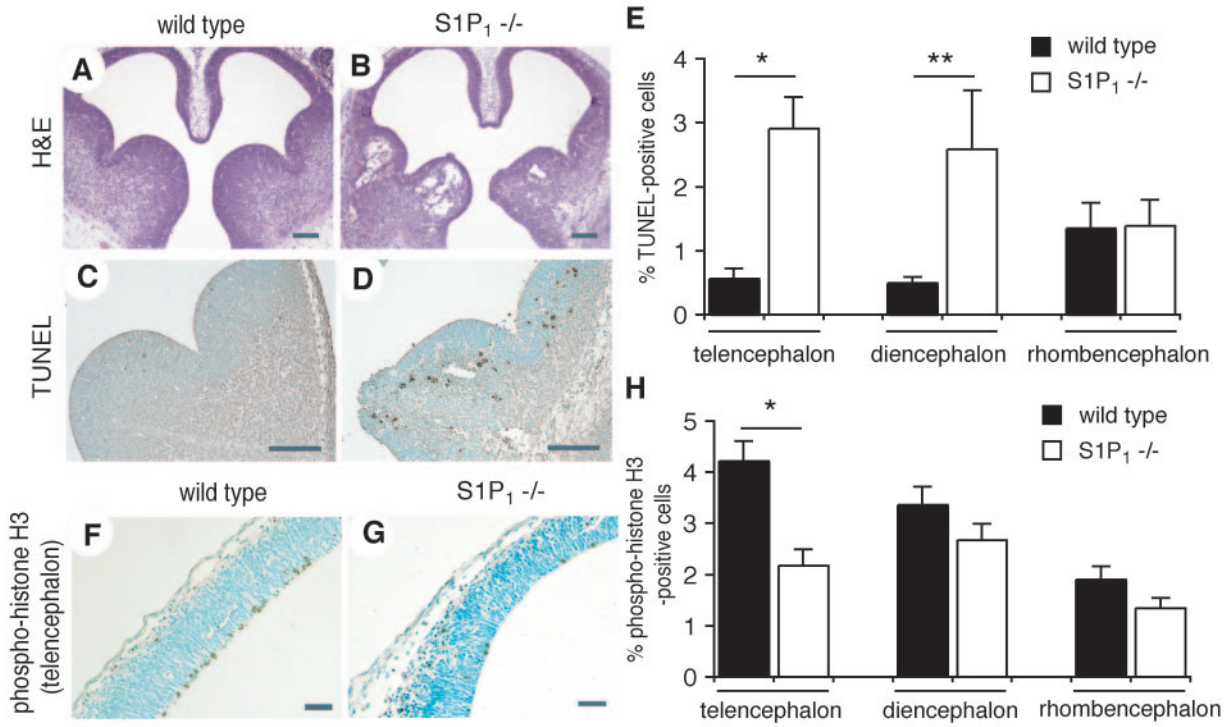

FIG. 6. Requirement of $S1P_1$ receptor for neural development. (A and B) H&E staining of transverse sections from wild-type (A) and $S1P_1^{-/-}$ mutant (B) embryos at E12.5. (C and D) TUNEL assay of wild-type (C) and $S1P_1^{-/-}$ mutant (D) embryos at E12.5. (E) Percentage of TUNEL-positive cells ($n = 6$ matched pairs; *, $P < 0.01$; **, $P < 0.05$ [paired t test]). (F and G) Immunostaining with anti-phospho-histone H3 of wild-type (F) and $S1P_1^{-/-}$ mutant (G) embryos at E12.5. (H) Percentage of phospho-histone H3-positive cells ($n = 6$ matched pairs; *, $P < 0.01$ [paired t test]). Scale bars represent 200 μm (A, B, C, and D) and 50 μm (F and G).

hibited NTDs, which are prevalent birth defects. More than 80 mutations that cause NTDs in mice have been reported, and alterations in cell survival and cell proliferation are frequently relevant to the NTDs (6). Indeed, our mutant mice showed increased cell death during neural tube closure periods, which may account for the NTDs. It has been reported that fumonisins, toxic and carcinogenic mycotoxins, disrupt sphingolipid metabolism and cause a high incidence of NTDs in mouse embryos in culture (20). It is noteworthy that substantial consumption of fumonisins is correlated with high incidences of NTDs in some regions of the world (20), indicating that disturbance of sphingolipid metabolism may be implicated in the pathogenesis of human NTDs. Thus, our mutant mice might be valuable animal models for common human NTDs.

The *SphK*-null mice revealed increased cell death and decreased cell proliferation in the neuroepithelial layer, with complete penetrance, even after neural tube closure periods, suggesting that those are general features induced by S1P-deficiency, irrespective of the presence of NTDs. It has been proposed that the effects of S1P on proliferation and suppression of apoptosis are mediated by both intracellular actions and S1P receptors (16, 23, 26, 27). Our results suggest that the effects of S1P on neural development are mediated, at least in part, by the $S1P_1$ receptor. The neural defects, demonstrated by increased cell death and decreased proliferation, in $S1P_1^{-/-}$ embryos were milder than those seen in $SphK1^{-/-}$ $SphK2^{-/-}$ embryos. Moreover, in contrast to $SphK1^{-/-}$ $SphK2^{-/-}$ embryos, we did not observe NTDs in $S1P_1^{-/-}$ embryos. These results indicate that perhaps other S1P receptors ($S1P_2$ to $S1P_5$) may be important participants in this pathway or that S1P may also act through an intracellular mechanism. Mice carrying multiple S1P receptor mutant alleles, such as $S1P_1^{-/-}$ $S1P_2^{-/-}$ and $S1P_1^{-/-}$ $S1P_3^{-/-}$ embryos, die earlier and show more severe vascular defects than do $S1P_1$ single mutants (14). It will be of interest to determine if the S1P receptors have synergistic effects on neurogenesis by analyzing the multiple S1P receptor mutants in more detail.

In summary, these findings demonstrate, for the first time, that S1P plays a critical role in neurogenesis during development through potent effects on neural cell survival and growth. It is noteworthy that S1P, clearly an angiogenic factor, is now implicated in neurogenesis, since it has been recently recognized that the two pathways, angiogenesis and neurogenesis, utilize some of the same molecules for their regulation (30). Furthermore, our findings raise the possibility that manipulation of the S1P/S1P receptor signaling pathway in the nervous system may provide novel therapeutic approaches in neurological disease through enhancement of neuronal survival, increasing proliferation of neural progenitors, or both.

ACKNOWLEDGMENTS

This research was supported by the Intramural Research Program of the NIH, NIDDK, and by NIH grant R 37 GM043880 (to S.S.). K.M. is supported by a JSPS Research Fellowship for Japanese Biomedical and Behavioral Researchers at NIH.

We have no competing financial interests.

REFERENCES

1. **Allende, M. L., T. Yamashita, and R. L. Proia.** 2003. G-protein-coupled receptor $S1P_1$ acts within endothelial cells to regulate vascular maturation. Blood **102:**3665–3667.
2. **Allende, M. L., J. L. Dreier, S. Mandala, and R. L. Proia.** 2004. Expression of the sphingosine-1-phosphate receptor, $S1P_1$, on T-cells controls thymic emigration. J. Biol. Chem. **279:**15396–15401.
3. **Allende, M. L., T. Sasaki, H. Kawai, A. Olivera, Y. Mi, G. van Echten-Deckert, R. Hajdu, M. Rosenbach, C. A. Keohane, S. Mandala, S. Spiegel, and R. L. Proia.** 2004. Mice deficient in sphingosine kinase 1 are rendered lymphopenic by FTY720. J. Biol. Chem. **279:**52487–52492.
4. **Bamforth, S. D., J. Bragança, J. Eloranta, J. N. Murdoch, F. I. Marques, K. R. Kranc, H. Farza, D. J. Henderson, H. C. Hurst, and S. Bhattacharya.** 2001. Cardiac malformations, adrenal agenesis, neural crest defects and exencephaly in mice lacking Cited2, a new Tfap2 co-activator. Nat. Genet. **29:**469–474.
5. **Cinamon, G., M. Matloubian, M. J. Lesneski, Y. Xu, C. Low, T. Lu, R. L. Proia, and J. G. Cyster.** 2004. Sphingosine 1-phosphate receptor 1 promotes B cell localization in the splenic marginal zone. Nat. Immunol. **5:**713–720.
6. **Copp, A. J., N. D. Greene, and J. N. Murdoch.** 2003. The genetic basis of mammalian neurulation. Nat. Rev. Genet. **4:**784–793.
7. **Coursol, S., L. M. Fan, H. Stunff, S. Spiegel, S. Gilroy, and S. M. Assmann.** 2003. Sphingolipid signaling in *Arabidopsis* guard cells involves heterotrimeric G proteins. Nature **423:**651–654.
8. **Cuvillier, O., G. Pirianov, B. Kleuser, P. G. Vanek, O. A. Coso, S. Gutkind, and S. Spiegel.** 1996. Suppression of ceramide-mediated programmed cell death by sphingosine-1-phosphate. Nature **381:**800–803.
9. **Edsall, L. C., and S. Spiegel.** 1999. Enzymatic measurement of sphingosine 1-phosphate. Anal. Biochem. **272:**80–86.
10. **Gowen, L. C., B. L. Johnson, A. M. Latour, K. K. Sulik, and B. H. Koller.** 1996. *Brca1* deficiency results in early embryonic lethality characterized by neuroepithelial abnormalities. Nat. Genet. **12:**191–194.
11. **Hla, T., M. J. Lee, N. Ancellin, J. H. Paik, and M. J. Kluk.** 2001. Lysophospholipids-receptor revelations. Science **294:**1875–1878.
12. **Igarashi, N., T. Okada, S. Hayashi, T. Fujita, S. Jahangeer, and S. Nakamura.** 2003. Sphingosine kinase 2 is a nuclear protein and inhibits DNA synthesis. J. Biol. Chem. **278:**46832–46839.
13. **Kohama, T., A. Olivera, L. Edsall, M. M. Nagiec, R. Dickson, and S. Spiegel.** 1998. Molecular cloning and functional characterization of murine sphingosine kinase. J. Biol. Chem. **273:**23722–23728.
14. **Kono, M., Y. Mi, Y. Liu, T. Sasaki, M. L. Allende, Y. P. Wu, T. Yamashita, and R. L. Proia.** 2004. The sphingosine-1-phosphate receptors $S1P_1$, $S1P_2$, and $S1P_3$ function coordinately during embryonic angiogenesis. J. Biol. Chem. **279:**29367–29373.
15. **Kupperman, E., S. An, N. Osborne, S. Waldron, and D. Y. Stainier.** 2000. A sphingosine-1-phosphate receptor regulates cell migration during vertebrate heart development. Nature **406:**192–195.
16. **Lee, M. J., S. Thangada, K. P. Claffey, N. Ancellin, C. H. Liu, M. Kluk, M. Volpi, R. I. Sha'afi, and T. Hla.** 1999. Vascular endothelial cell adherens junction assembly and morphogenesis induced by sphingosine-1-phosphate. Cell **99:**301–312.
17. **Liu, H., M. Sugiura, V. E. Nava, L. C. Edsall, K. Kono, S. Poulton, S. Milstien, T. Kohama, and S. Spiegel.** 2000. Molecular cloning and functional characterization of a novel mammalian sphingosine kinase type 2 isoform. J. Biol. Chem. **275:**19513–19520.
18. **Liu, Y., R. Wada, T. Yamashita, Y. Mi, C. X. Deng, J. P. Hobson, H. M. Rosenfeldt, V. E. Nava, S. S. Chae, M. J. Lee, C. H. Liu, T. Hla, S. Spiegel, and R. L. Proia.** 2000. Edg-1, the G-protein-coupled receptor for sphingosine-1-phosphate, is essential for vascular maturation. J. Clin. Investig. **106:**951–961.
19. **Liu, H., R. E. Toman, S. K. Goparaju, M. Maceyka, V. E. Nava, H. Sankala, S. G. Payne, M. Bektas, I. Ishii, J. Chun, S. Milstien, and S. Spiegel.** 2003. Sphingosine kinase type 2 is a putative BH3-only protein that induces apoptosis. J. Biol. Chem. **278:**40330–40336.
20. **Marasas, W. F., R. T. Riley, K. A. Hendricks, V. L. Stevens, T. W. Sadler, J. Gelineau-van Waes, S. A. Missmer, J. Cabrera, O. Torres, W. C. Gelderblom, J. Allegood, C. Martínez, J. Maddox, J. D. Miller, L. Starr, M. C. Sullards, A. V. Roman, K. A. Voss, E. Wang, and A. H. Merrill, Jr.** 2004. Fumonisins disrupt sphingolipid metabolism, folate transport, and neural tube development in embryo culture and in vivo: a potential risk factor for human neural tube defects among populations consuming fumonisin-contaminated maize. J. Nutr. **134:**711–716.
21. **Matloubian, M., C. G. Lo, G. Cinamon, M. J. Lesneski, Y. Xu, V. Brinkmann, M. L. Allende, R. L. Proia, and J. G. Cyster.** 2004. Lymphocyte egress from thymus and peripheral lymphoid organs is dependent on S1P receptor 1. Nature **427:**355–360.
22. **McGiffert, C., J. J. Contos, B. Friedman, and J. Chun.** 2002. Embryonic brain expression analysis of lysophospholipid receptor genes suggests roles for $s1p_1$ in neurogenesis and $s1p_{1-3}$ in angiogenesis. FEBS Lett. **531:**103–108.
23. **Morita, Y., G. I. Perez, F. Paris, S. R. Miranda, D. Ehleiter, A. Haimovitz-Friedman, Z. Fuks, Z. Xie, J. C. Reed, E. H. Schuchman, R. N. Kolesnick, and J. L. Tilly.** 2000. Oocyte apoptosis is suppressed by disruption of the *acid sphingomyelinase* gene or by sphingosine-1-phosphate therapy. Nat. Med. **6:**1109–1114.
24. **Olivera, A., and S. Spiegel.** 1993. Sphingosine-1-phosphate as second messenger in cell proliferation induced by PDGF and FCS mitogens. Nature **365:**557–560.
25. **Olivera, A., T. Kohama, Z. Tu, S. Milstien, and S. Spiegel.** 1998. Purification and characterization of rat kidney sphingosine kinase. J. Biol. Chem. **273:** 12576–12583.
26. **Olivera, A., T. Kohama, L. Edsall, V. Nava, O. Cuvillier, S. Poulton, and S. Spiegel.** 1999. Sphingosine kinase expression increases intracellular sphingosine-1-phosphate and promotes cell growth and survival. J. Cell Biol. **147:**545–558.
27. **Olivera, A., H. M. Rosenfeldt, M. Bektas, F. Wang, I. Ishii, J. Chun, S. Milstien, and S. Spiegel.** 2003. Sphingosine kinase type 1 induces $G_{12/13}$-mediated stress fiber formation, yet promotes growth and survival independent of G protein-coupled receptors. J. Biol. Chem. **278:**46452–46460.
28. **Ruland, J., G. S. Duncan, A. Elia, I. del Barco Barrantes, L. Nguyen, S. Plyte, D. G. Millar, D. Bouchard, A. Wakeham, P. S. Ohashi, and T. W. Mak.** 2001. Bcl10 is a positive regulator of antigen receptor-induced activation of NF-κB and neural tube closure. Cell **104:**33–42.
29. **Spiegel, S., and S. Milstien.** 2003. Sphingosine-1-phosphate: an enigmatic signaling lipid. Nat. Rev. Mol. Cell Biol. **4:**397–407.
30. **Storkebaum, E., D. Lambrechts, and P. Carmeliet.** 2004. VEGF: once regarded as a specific angiogenic factor, now implicated in neuroprotection. Bioessays **26:**943–954.
31. **Wilkinson, D. G.** 1992. *In situ* hybridization: a practical approach. IRL Press, Oxford, United Kingdom.